Guanidinylated apolipoprotein C3 (ApoC3) causes cardiovascular and kidney injury

Authors

Stefan J. Schunk, MD[1]; Juliane Hermann, PhD[2]; Sarah Triem, MSc[1]; Tamim Sarakpi, MD[1]; Michaela Lellig, PhD[2]; Eunsil Hahm, PhD[3]; Stephen Zewinger, MD[1]; Julia Möllmann, PhD[4]; Michael Lehrke, MD[4]; Rafael Kramann, MD PhD[5]; Peter Boor MD PhD[6]; Peter Lipp, PhD[7]; Ulrich Laufs, MD[8]; Jochen Reiser, MD PhD[3]; Joachim Jankowski, PhD[2,9]; Danilo Fliser, MD[1]; Thimoteus Speer, MD PhD[1,10]; Vera Jankowski, PhD[2]

Affiliations

1 Saarland University, Department of Internal Medicine IV, Nephrology and Hypertension, Homburg/Saar, Germany

2 RWTH Aachen University Hospital, Institute of Molecular Cardiovascular Research, Aachen, Germany

3 Rush University Medical Center, Department of Internal Medicine, Chicago, IL, USA

4 RWTH Aachen University Hospital, Department of Cardiology, Aachen, Germany

5 RWTH Aachen University Hospital, Department of Nephrology, Aachen, Germany

6 RWTH Aachen University Hospital, Institute of Pathology, Aachen, Germany

7 Saarland University, Institute of Cell Biology, PZMS, Homburg/Saar, Germany

8 University Hospital Leipzig, Department of Cardiology, Leipzig, Germany

9 Maastricht University, School for Cardiovascular Diseases, Maastrich, The Netherlands

10 Saarland University, Translational Cardio-Renal Medicine, Homburg/Saar, Germany

Corresponding author and lead contact

Thimoteus Speer, MD PhD

Saarland University

Translational Cardio-Renal Medicine and Department of Internal Medicine IV

Nephrology and Hypertension

Kirrberger Strasse, Building 41

66421 Homburg/Saar

Phone: +49 6841 16 15048

Fax: +49 6841 16 17 21503

E-Mail: timo.speer@uks.eu

Word count: 23,566 characters (excluding methods and references)

Keywords: Inflammation, lipoproteins, posttranslational modifications, cardiovascular disease, myocardial infarction, chronic kidney disease

Abstract

Cardiovascular diseases (CVD) and chronic kidney diseases (CKD) are highly prevalent in Western populations and account for a substantial proportion of mortality. We found that apolipoprotein C-3 (ApoC3), a constituent of triglyceride-rich lipoproteins, induces alternative NLRP3 inflammasome activation in human monocytes and thus causes sterile inflammation. Here, we describe posttranslational guanidinylation of lysine residues of ApoC3 (gApoC3) in patients after acute myocardial infarction and in patients with CKD, that augments the proinflammatory effects of ApoC3. gApoC3 accumulates in kidneys and hearts after injury as determined by 2D-proteomic analyses, and further promotes tissue damage in humanized mice. In a prospective clinical trial of 543 patients, higher gApoC3 blood levels as determined by mass spectrometry were associated with increased mortality as well as cardiovascular and renal events. Therefore, guanidinylation of ApoC3 represents a common pathogenic mechanism in CKD and CVD, rendering gApoC3 a potential therapeutic target.

Introduction

Chronic kidney disease (CKD) represents one of the strongest risk factors for cardiovascular diseases (CVD) (Chronic Kidney Disease Prognosis Consortium et al., 2010). Vice versa, CVD such as hypertension promote the development and progression of CKD in a vicious circle (Ortiz et al., 2014). CVD and CKD are highly prevalent in the Western population. Between 2005 and 2015, the prevalence of CKD and ischemic heart disease increased by more than 25 % rendering both diseases global public health problems (G. B. D. Disease Injury Incidence Prevalence Collaborators, 2018). The mechanisms promoting CVD in patients with CKD are complex and yet only partially understood. Moreover, specific links between both organs remain widely elusive.

It is known that an altered lipoprotein profile promotes CKD-associated CVD (Speer et al., 2013b). High-density lipoprotein (HDL) from CKD patients not only loses its vasoprotective properties but turns into a noxious agent promoting endothelial dysfunction, hypertension and atherosclerosis (Speer et al., 2014b; Zewinger et al., 2014). Mechanistically, we found that HDL from CKD patients is structurally modified compared to HDL from healthy subjects by the accumulation of small molecules such as symmetric dimethylarginine (SDMA), changes of its protein composition, and posttranslational protein modifications (PTMs) (Speer et al., 2013a; Zewinger et al., 2015; Zewinger et al., 2017). Thereby, CKD-dependent factors such as urea, but also CKD-independent factors such as inflammation-dependent myeloperoxidase induce PTM of apolipoproteins in HDL and low-density lipoprotein (LDL) as well (Wang et al., 2007). One of these PTMs, occurring mostly in CKD patients, represents the carbamylation of lysine residues. Carbamylated LDL promotes endothelial dysfunction and its plasma concentrations are associated with adverse clinical outcomes (Speer et al., 2014a). Therefore, PTMs of proteins and peptides have broad consequences on the functionality of (apo)lipoproteins (Gajjala et al., 2015).

Recently, we found that apolipoprotein C3 (ApoC3), the major protein constituent of triglyceride-rich lipoproteins such as very low-density lipoprotein (VLDL), induces sterile systemic inflammation by activating the NOD-like receptor protein-3 (NLRP3) inflammasome

in human monocytes via an alternative pathway (Zewinger et al., 2020). This finding has important pathophysiological consequences. ApoC3 induces the release of the NLRP3-dependent proinflammatory cytokine interleukin-1β (IL-1β) in a concentration-dependent manner, which impedes the regeneration of injured arterial vessels and promotes the development of kidney damage. This is of importance for all clinical conditions associated with increased plasma levels of ApoC3 such as CKD, coronary artery disease, myocardial infarction, and diabetes mellitus.

The present study aimed to assess the PTMs of ApoC3 in patients with prevalent CVD and CKD and to determine the effects of posttranslationally modified ApoC3 *in vitro* and *in vivo*. Finally, we tested the relevance of such PTMs of ApoC3 in a prospective clinical trial.

Results

Identification of posttranslational modifications (PTMs) of ApoC3

ApoC3 from healthy subjects, patients with CKD, and patients with acute myocardial infarction (AMI) was subjected to proteomic analyses. We detected posttranslational guanidinylation of ApoC3 from patients with CKD and AMI but not of ApoC3 from healthy subjects (**Figure 1A+B**). Guanidinylation was found at four different lysine sites (Lys41, 44, 78, 80, **Figure 1C**). *Ex vivo*, guanidinylation of ApoC3 could have been induced by incubation of ApoC3 with methylisourea (**Figure 1D**). This guanidinylated ApoC3 (gApoC3). preparation was used for all subsequent *in vitro* and *in vivo* assays. To determine biologically relevant pathways leading to posttranslational guanidinylation, ApoC3 was incubated with either guanidine or urea. While guanidine induced guanidinylation of lysine residues, incubation of ApoC3 with urea led to guanidinylation and carbamylation of lysine as well (**Figure 1D+E**).

Guandinylated ApoC3 promotes inflammation

Since ApoC3 induces NLRP3 inflammasome-dependent pro-inflammatory activation of human monocytes (Zewinger et al., 2020), we performed *ex vivo* guanidinylation of ApoC3 and incubated human monocytes with native (nApoC3, i.e. unmodified ApoC3) or gApoC3. We found that gApoC3 induces significantly higher release of IL-1β and IL-6 as compared to nApoC3 (**Figure 2A+B**). Mechanistically, we have previously shown that exaggerated production of reactive oxygen species (ROS) is responsible for ApoC3-mediated alternative NLRP3 activation (Zewinger et al., 2020). Therefore, we quantified ROS production in human monocytes (**Figure 2C**). gApoC3 led to a significantly higher ROS production as compared to nApoC3, which might explain the more pronounced pro-inflammatory properties of gApoC3 in comparison to nApoC3. Notably, guanidinylation enhanced the binding of Atto-488-labeled ApoC3 to human monocytes (**Figure 2D**). To determine the effect of guanidinylation on the binding of ApoC3 on TLR2 or TLR4, which mediate the pro-inflammatory properties of ApoC3 (Zewinger et al., 2020), HEK cells stably expressing *Tlr2* or *Tlr4* were incubated with

fluorescent-labeled nApoC3 or gApoC3 (**Figure 2E**). Guanidinylation enhanced the binding of ApoC3 to TLR4, whereas binding to TLR2 was similar with nApoC3 or gApoC3.

Guandinylated ApoC3 accumulates in hearts and kidneys after injury

To assess on whether gApoC3 accumulates within tissues after organ damage, we performed 2D-proteomic analyses of heart and kidney sections. We detected gApoC3 at a 1113.6 m/z (intensive green-yellow area) in the myocardium of mice after experimental ligation of the left anterior descending coronary artery, a mouse model for AMI (**Figure 3A**). gApoC3 accumulation was present already seven days after AMI and still detectable 28 days after AMI. Interestingly, in an overlay of the mass-spectrometry images with Gomori-Trichrome stained hearts, gApoC3 was not only detectable within the scarring tissue but also subpericardial and subendocardial (**Figure 3B**). In mice subjected to a sham procedure, no relevant gApoC3 accumulation in cardiac tissue was present.

Similarly, we found gApoC3 accumulation in kidneys of mice subjected to an adenine diet as a murine model of CKD (**Figure 3C**). In contrast, gApoC3 was not detectable in the kidneys of mice fed with a normal chow diet. These findings indicate that AMI and CKD both induce the guanidinylation of ApoC3, which subsequently accumulates within the injured organs.

Guandinylated ApoC3 impedes vascular regeneration and promotes kidney injury

Next, we assessed the effects of gApoC3 on vascular and kidney injury *in vivo*. We have shown that ApoC3 mediates alternative NLRP3 activation, a pathway restricted to human monocytes only (Zewinger et al., 2020). We therefore subjected humanized mice, i.e. immune-incompetent mice transplanted with human monocytes, to perivascular carotid artery injury, a model for vascular regeneration (**Figure 4A**). In this model, gApoC3 suppressed re-endothelialization of the carotid artery to a significantly greater extent as compared to nApoC3 (**Figure 4B+C**).

Additionally, we performed unilateral ureteral ligation – a model of kidney fibrosis – in humanized mice reconstituted with human monocytes (**Figure 4D**). Whereas nApoC3 had almost no effect on the development of kidney fibrosis, gApoC3 significantly enhanced kidney fibrosis five days after injury (**Figure 4E-F**). We found a higher accumulation of macrophages (F4/80) and neutrophils (Ly6G) within the kidneys after treatment with gApoC3 as compared to nApoC3 (**Figure 4G-H**). Furthermore, kidney tissue expression of the tubular epithelial cell stress marker Dickkopf-3 (DKK3) was significantly greater in mice after injection of gApoC3 in comparison to mice receiving nApoC3 (**Figure 4I**). This indicates that guanidinylation augments the adverse effects of ApoC3 on vascular regeneration and kidney injury.

Guanidinylated ApoC3 is associated with cardiovascular and renal outcomes

To assess the clinical relevance of these experimental findings, we quantified posttranslational guanidinylation of ApoC3 (gApoC3 intensity) in plasma samples from 543 patients included in the prospective CARE FOR HOME study, representing CKD patients at high cardiovascular risk. Baseline characteristics are shown in **Table S1**. The ApoC3 guanidinylation mass-signal intensity was not associated with an altered lipoprotein phenotype (**Figure S1A-E**), but with higher systemic inflammation, i.e. higher high sensitivity C-reactive protein (**Figure S1F**). Importantly, the guanidinylation of ApoC3 was higher in subjects with prevalent CAD or higher CKD stage, i.e. more advanced reduction of estimated glomerular filtration rate (eGFR), but not in patients with other cardiovascular risk factors such as smoking or diabetes mellitus (**Figure S1G**).

To model the association between the gApoC3 mass-signal intensity and the risk of the combined cardiovascular endpoint and all-cause mortality we used restricted cubic splines. A higher ApoC3 mass guanidinylation mass-signal intensity was significantly associated with a higher risk of the combined cardiovascular endpoint (**Figure 5A**) and all-cause mortality (**Figure 5B**, $P<0.0001$ for each endpoint). This association was independent of several confounding covariates including eGFR, albuminuria, and triglyceride plasma concentration. These findings were confirmed in Cox regression models using gApoC3 mass-signal intensity

divided into tertiles (**Tables S2-3**). Importantly, neither triglycerides nor ApoC3 plasma levels did associate with the CV endpoint or all-cause mortality (**Tables S4-7**).

Next, the association between gApoC3 mass-signal intensity and the combined renal endpoint (i.e. 50 % eGFR reduction, end-stage kidney disease, and death) was determined (**Figure 5C**). Higher gApoC3 mass-signal intensity was associated with a higher risk of reaching the combined renal endpoint. This association was independent of baseline kidney function (i.e. eGFR), albuminuria, and other covariates including triglycerides (**Table S8**). Again, triglycerides or ApoC3 blood levels were not associated with the combined renal endpoint (**Table S9-10**).

In the CARE FOR HOME trial, eGFR has been determined at baseline as well as at annual follow-up visits. Changes of eGFR during follow-up were modeled using group-based trajectory modeling (**Figure 5D**). Using this approach, we identified four different patterns of eGFR. While eGFR remained stable in 132 patients (23.1 %), 339 participants (59.0 %) were characterized by declining eGFR and 92 participants (16.1 %) by rapidly declining eGFR during follow-up. Higher baseline gApoC3 mass-signal intensity was associated with a significantly higher risk for assignment to the group of patients with declining or rapidly declining kidney function (**Figure 5E**, **Table S11**).

Discussion

We identified the guanidinylation of ApoC3 as a novel posttranslational protein modification in patients with CKD as well as in patients with AMI. Experimental data and analyses in a large prospective clinical trial highlight gApoC3 as a mediator of more intense (cardio)vascular and kidney injury. Thus, targeting ApoC3 or its guanidinylation has the potential to serve as a therapeutic target at the cardio-renal interaction.

ApoC3 plays an important role in the metabolism of triglyceride-rich lipoproteins mainly by inhibiting lipoprotein lipase and hepatic lipase leading to hypertriglyceridemia (Gordts et al., 2016). Carriers of null mutations in *APOC3* are characterized by lower levels of triglycerides, higher HDL-C, and lower LDL-C (Pollin et al., 2008). Subsequently, large genetic-association studies revealed an association between loss-of-function mutations in *APOC3* and a lower risk of ischemic vascular disease (Jorgensen et al., 2014) and CAD (TG and HDL Working Group of the Exome Sequencing Project et al., 2014). Moreover, ApoC3 present in HDL has been documented to abolish its vasoprotective properties (Jensen et al., 2018; Morton et al., 2018).

ApoC3 is not only relevant during the pathogenesis of CVD, it is also involved in the evolution of the metabolic syndrome and of CKD. *APOC3* gain-of-function variants are associated with non-alcoholic fatty liver disease, insulin resistance (Petersen et al., 2010), and with worse outcomes in patients with CKD (Zewinger et al., 2020). Besides that, ApoC3 triggers a pro-coagulatory response (Martinelli et al., 2019) and links islet insulin resistance to β-cell failure in diabetes (Avall et al., 2015). Recent evidence suggests that ApoC3 directly interacts with endothelial cells and monocytes to drive an inflammatory response (Zewinger et al., 2020; Zheng et al., 2013). We previously found that ApoC3 induces activation of the NLRP3 inflammasome in human monocytes by targeting alternative NLRP3 activation leading to sterile systemic inflammation, impaired vascular regeneration, and kidney damage (Zewinger et al., 2020). In the present study, gApoC3 was not associated with an altered lipoprotein profile, but with increased sterile systemic inflammation as shown by higher high-sensitivity C-reactive protein plasma levels in subjects with more intense guanidinylation of ApoC3. This points to diverse effects of native and posttranslationally modified ApoC3. Guanidinylation of

ApoC3 mainly modulates its pro-inflammatory properties as determined by an increased release of the pro-inflammatory cytokines IL-1β and IL-6 from monocytes as compared to nApoC3. gApoC3 also promotes the production of ROS by monocytes, which we recently documented to mediate alternative NLRP3 activation (Zewinger et al., 2020). Mechanistically, we found that guanidinylation increases the binding of ApoC3 to TLR4, which mediates the adverse effects of ApoC3 on the monocyte pro-inflammatory state together with TLR2 (Zewinger et al., 2020). This is in line with previous studies demonstrating that other PTMs such as oxidation or carbamylation of e.g. LDL affect its protein structure and the ability to bind to certain cell surface receptors (Wang et al., 2007; Wolska et al., 2020).

Posttranslational guanidinylation has been recently identified in patients with CKD (Rueth et al., 2015; Schuett et al., 2017) and in patients with systemic lupus erythematodes (SLE) (Breitkopf et al., 2020). Guanidinylated albumin shows a decreased binding capacity of hydrophobic metabolites (Rueth et al., 2015) and guanidinylated fibrinogen promotes a denser fibrin clot structure in patients on hemodialysis (Schuett et al., 2017). Moreover, the guanidinylation of Y-box binding protein1 (YB-1) in SLE results in enhanced Notch-3 signaling in T lymphocytes (Breitkopf et al., 2020). In this study, we describe guanidinylation of ApoC3 in patients with CKD as well as in patients with AMI as well. In addition, gApoC3 was detected in a CKD animal model and in experimental myocardial infarction. We found that guanidine, which is elevated in the plasma of patients with CKD, diabetes mellitus, heart failure and after endotoxin challenge (Cullen et al., 2006; Deshmukh et al., 1997; Urpi-Sarda et al., 2019), as well as urea, which accumulates in the blood of CKD patients, drive guanidinylation of ApoC3 *ex vivo*. While urea induces guanidinylation and carbamylation, guanidine only mediates guanidinylation of ApoC3.

We confirmed the relevance of this protein modification in a large-scale prospective clinical study, in which proteomic analyses of ApoC3 were performed in 543 individuals with confirmed CKD. The findings highlight guanidinylation as an important therapeutic target in clinical conditions characterized by elevated ApoC3 and enhanced protein guanidinylation, e.g. in CKD, CAD, or inflammatory states (e.g. SLE). Several approaches to lower ApoC3 are

currently under clinical evaluation. It has been shown that antisense nucleotides targeting ApoC3 reduce plasma triglycerides (Graham et al., 2013) in patients with hypertriglyceridemia and familial chylomicronemia syndrome (Gaudet et al., 2015; Gaudet et al., 2014). In a phase III clinical trial, the *APOC3*-targeting anti-sense nucleotide Volanesorsen reduced ApoC3 plasma levels by 84% without serious adverse events (Witztum et al., 2019). Similarly, monoclonal antibodies for the inhibition of ApoC3 (Khetarpal et al., 2017) or ApoC3 antagonist peptides are in development (Wolska et al., 2020). Based on our findings, these agents might not only be of relevance for the treatment of hypertriglyceridemia but also as a tool to prevent ApoC3-induced (micro)inflammation and organ damage in patients with CKD, CAD, diabetes, and other inflammatory disorders.

Several limitations of our clinical study have to be considered. It has been performed in a cohort of Caucasian ancestry and can therefore not be generalized to other ethnicities. Moreover, the development of a specific treatment inhibiting ApoC3 guanidinylation should be the subject of future studies. Therefore, we are not able to prove that therapeutic targeting of ApoC3 guanidinylation has definite beneficial clinical effects.

Taken together, the present study provides evidence from preclinical models and a prospective clinical trial that gApoC3 plays an important role in the development of organ injury in patients with CKD, AMI and other clinical conditions. The clinical study represents one of the largest trials, in which the association of a specific PTM and clinically relevant outcomes was assessed. These findings highlight gApoC3 as a pathophysiologically relevant factor in development of organ dysfunction. Thus, prevention of the guanidinylation of ApoC3 and other proteins might represent a novel therapeutic approach.

Acknowledgments

Funded by the Deutsche Forschungsgemeinschaft (DFG, German Research Foundation) – SFB TRR 219 – Project-ID 322900939.

Author contributions

Conceptualization, SJS, EH, JR, JJ, DF, TS, VJ; Methodology, SJS, ST, TSa, ML, EH, SZ, JJ, DF, TS, VJ; Formal Analysis, SJS, JH, ST, TSa, SZ, ML, JM, ML, RK, PB, PL, UL, TS, VJ; Investigation, SJS, JH, ST, ML, EH, JM, ML, RK, PB, PL, UL, TS, VJ; Resources, SJS, EH, JM, ML, JR, TS, VJ. Writing – Original Draft, SJS, DF, TS, VJ. Writing – Review & Editing, JH, ST, TSa, ML, EH, SZ, JM, ML, RK, PB, PL, UL, JR, JJ. Visualization, SJS, JH, ST, TS, VJ. Funding Acquisition, DF, TS, VJ. Supervision: SJS, DF, TS, VJ.

Declaration of interests

The authors declare no competing interests.

Figure legends

Figure 1

Guanidinylation of ApoC3 in patients with chronic kidney diseases (CKD) or in patients with acute myocardial infarction (AMI).

A Characteristic MALDI-TOF mass spectra of native ApoC3 (i.e. unmodified ApoC3) and ApoC3 from a healthy subject, a patient with CKD, and a patient with AMI, respectively. Red arrows indicate guanidinylated Lysine 44.

B Number of guanidinylated lysine residues in healthy subjects, and in patients with CKD or in patients with AMI (N=5).

C Three-dimensional structure of human ApoC3 with lysine residues marked, at which posttranslational guanidinylation was detected.

D Characteristic MALDI-TOF mass spectra of plasma incubated with methylisourea, guanidine, or urea.

E Chemical pathways inducing guanidinylation or carbamylation of lysine residues in ApoC3.

Figure 2

Guandinylated ApoC3 induces inflammation.

A Release of IL-1β in the supernatant of human monocytes incubated with LPS (10 ng/mL), nApoC3 or gApoC3 (50 µg/mL, 16 hr, N=6 per group).

B Release of IL-6 in the supernatant of human monocytes incubated with LPS (10 ng/mL), nApoC3 or gApoC3 (50 µg/mL, 16 hr, N=6 per group).

C Superoxide production of human monocytes incubated with LPS (10 ng/mL), nApoC3 or gApoC3 (50 µg/mL, 1 hr, N=6 per group).

D Binding of Atto-488-labeled nApoC3 or gApoC3 (1 hr) to human monocytes as determined by flow cytometry. Representative of at least three independent experiments.

E Fluorescence intensity of HEK cells transfected with *Tlr2* or *Tlr4* constructs incubated with Atto-488-labeled nApoC3 or gApoC3 for 1 hr. Representative of at least three independent experiments.

Data are represented as mean ± SEM.

Figure 3

Guandinylated ApoC3 accumulates after kidney injury and myocardial infarction.

A Representative 2D-proteomic images showing the guanidinylated ApoC3 fragment FLK*GYWSK* (m/z 1113.6) in hearts of mice subjected to LAD ligation or sham surgery after 7 days and 28 days. Representative of at least three independent experiments.

B Overlay of Gomori-Trichrome stained myocardial tissue sections with 2D-proteomic images showing the guanidinylated ApoC3 fragment FLK*GYWSK* (m/z 1113.6) in hearts of mice subjected to LAD ligation or sham surgery 7 days or 28 days after the surgery. Representative of at least three independent experiments.

C Representative 2D-proteomic images showing the guanidinylated ApoC3 fragment FLK*GYWSK* (m/z 1113.6) in mice subjected to an adenine diet or control chow diet for 14 days. Representative of at least three independent experiments.

Figure 4

Guanidinylated ApoC3 induces vascular and kidney injury in humanized mice.

A Schematic of the perivascular carotid injury model.

B-C Re-endothelialized areas at 1 week after perivascular carotid injury in NOD-SCID mice injected with nApoC3 or gApoC3 (50 µg/mL blood volume, N=6 per group).

D Schematic of the unilateral ureter ligation model.

E-F Kidney fibrosis as determined by Sirius red staining in kidneys of NOD-SCID mice 5 days after unilateral ureter ligation and injection with nApoC3 or gApoC3 (50 µg/mL blood volume, N=4-5 per group).

G Renal expression of F4/80 5 days after unilateral ureter ligation (N=4-5 per group).

H Renal expression of Ly6G 5 days after unilateral ureter ligation (N=4-5 per group).

I Renal expression of DKK3 5 days after unilateral ureter ligation (N=4-5 per group).

Data are represented as mean ± SEM.

Figure 5

Guandinylated ApoC3 associates with cardiovascular and renal outcomes.

A Restricted cubic spline plots of the association between gApoC3 mass-signal intensity and the risk of the combined cardiovascular endpoint in 543 subjects included in the prospective CARE FOR HOMe study. The red line indicates the risk for the combined cardiovascular endpoint with respective 95% CIs (light grey area). Blue spikes show the individual distribution of gApoC3 mass-signal intensity.

B Restricted cubic spline plots of the association between gApoC3 mass-signal intensity and the risk of mortality in 543 subjects included in the prospective CARE FOR HOMe study. The red line indicates the risk for mortality with respective 95% CIs (light grey area). Blue spikes show the individual distribution of gApoC3 mass-signal intensity.

C Restricted cubic spline plots of the association between gApoC3 mass-signal intensity and the risk of the combined renal endpoint in 543 subjects included in the prospective CARE FOR HOMe study. The red line indicates the risk for the combined renal endpoint with respective 95% CIs (light grey area). Blue spikes show the individual distribution of gApoC3 mass-signal intensity.

D Group-based trajectory modeling of change of eGFR in 543 participants of the prospective CARE FOR HOMe study. Gray-shaded area represents 95 % confidence intervals.

E Association of gApoC3 mass-signal intensity and eGFR trajectory groups.

All plots are adjusted for age, sex, prevalent cardiovascular disease, body mass index, systolic blood pressure, smoking status, diabetes mellitus, estimated glomerular filtration rate (kindey function), and albuminuria.

See also Figure S1

STAR methods

Key resources tables

REAGENT or RESOURCE	SOURCE	IDENTIFIER
Antibodies		
F4/80 Monoclonal Antibody (BM8)	eBioscience	#14-4801-82
Ly6G/Ly6C Monoclonal Antibody (RB6-8C5)	eBioscience	#14-5931-82
Anti-DKK3 Antibody	Abcam	#ab187532
Goat anti-Rat IgG (H+L) Secondary Antibody, Biotin	Invitrogen	#31830
Goat anti-Rabbit IgG (H+L) Secondary Antibody, Biotin	Invitrogen	#31820
Chemicals, Peptides, Recombinant Proteins		
CMH	Noxygen	#NOX-02.1-50mg
ApoC3	Hölzel Diagnostika	#33P-110
Atto-488 NHS-Ester	Atto-Tec	#AD 488-31
Vectashield Hard Set Antifade Mounting Medium with DAPI	Vector Laboratories	#H-1500-10
Critical Commercial Assays		
Human IL-1beta/IL-1F2 Duoset ELISA	R&D systems	#DY201
Human IL-6 Duoset ELISA	R&D systems	#DY206
CD14 MicroBeads, Human	Miltenyi Biotec	#130-050-201
Critical Commercial Assays		

Human IL-1beta/IL-1F2 Duoset ELISA	R&D systems	#DY201
Experimental Models: Cell Lines		
HEK-Blue hTLR2 cells	Invivogen	#hkb-htlr2
HEK-Blue hTLR4 cells	Invivogen	#hkb-htlr4
Experimental Models: Organisms/Strains		
NOD.CB17/Prkdcscid/scid/Rj	Janvier	
Software		
SPSS Statistics Version 25	IBM	
Stata/IC 15.1	StataCorp	
Prism 8 for macOS	GraphPad Software	
Image J 1.52a	National Institutes of Health	
ZEN 3.0 (blue edition)	Carl Zeiss Microscopy	
WinEPR Aquistion Program	Bruker BioSpin	

Resource Availability

Lead Contact

Further information and requests for resources and reagents should be directed and will be fulfilled by the Lead Contact, Thimoteus Speer (timo.speer@uks.eu).

Materials Availability

This study did not generate new unique reagents.

Experimental Model and Subject Details

Mice

NOD.CB17/Prkdcscid/scid/Rj mice were purchased from Janvier and housed in individual cages kept at the animal facility at Saarland University Hospital. All animal experiments were approved by the Veterinary Office of Saarland, Germany.

CARE FOR HOME study

The CARE FOR HOME study comprises stable patients with confirmed CKD recruited at the outpatient clinic of the Saarland University Medical Center. The study was approved by the local Ethics Committee and all participants gave their written consent. The study design has been described previously in detail (Zewinger et al., 2018). Briefly, the study enrolled patients with CKD stage 2-4 according to the KDIGO guidelines aged ≥18 years (KDIGO, 2012). Patient with active malignant diseases, clinically apparent infections, active immunosuppressive therapy, kidney transplantation, and confirmed acute kidney injury were excluded. 543 participants were included in the present analyses. The median follow-up time was 5.3 years (IQR 4.0 years). In addition, patients were invited for annual follow-up assessments, were eGFR was determined. Plasma samples for proteomic analyses were obtained after overnight fasting and samples were immediately processed and stored at -80 °C until analyses. The combined cardiovascular endpoint was defined as an atherosclerotic disease event or death. The combined renal endpoint comprised 50 % decline of eGFR, requirement of renal replacement therapy, or death.

Cell lines

HEK293 cells co-transfected with human *Tlr2* or *Tlr4* genes were purchased from Invivogen. Cells were cultured in DMEM medium containing 4.5 g/l glucose, 10 % FBS, 50 U/ml penicillin, 50 µg/ml streptomycin, 100 µg/ml Normocin (Invivogen) and 2 mM L-glutamine.

Methods Details

Mass spectrometry and proteomic analyses

30 µg protein was separated by SDS-polyacryamide gel electrophoresis. Proteins were stained using Commassie Brilliat Blue G-250 (BioRad, Munich, Germany). The gel plugs were

manually separated in 0-20 kDa and 20-37 kDa the Gel plugs were washed and equilibrated, respectively, by using ammonium bicarbonate in acetonitrile. The isolated proteins was digested by trypsin and analyzed by matrix-assisted-laser-desorption/ionization-time of flight-mass spectrometer (MALDI-TOF-TOF) (Kork et al., 2018; Rueth et al 2015) Briefly the protein plugs were incubated with ammonium bicarbonate (50 mM) and 0.03% w/C trypsin for 24h at 37°C. The resulting tryptic peptides were desalted and concentrated by using $ZipTip_{C18}$ technology (Millipore, Billerica, MA, USA) and eluted with 80% acetonitrile directly onto the (MALDI) target plate (MTP-Ground steel 400/384; Bruker Daltonic) using alpha-cyano-4-hydrocinnamic acid as MALDI matrix and C13. The subsequent mass-spectrometric (MS) analyses were performed using both a MALDI-time of flight/time of flight (TOF/TOF) mass spectrometer (Ultraflex III; Bruker-Daltonic, Germany) and a MALDI-RapifleX mass-spectrometer (Bruker-Daltonic, Germany). The MALDI-TOF/TOF instrument was equipped with a smart-beam laser operated at a repetition rate of 100–200 Hz. The presented spectra are the representative average spectra with sum of 200 single-shot spectra for MS mode. The positively charged ions mass-spectra were analyzed in the reflector mode using delayed ion-extraction.

Analysis of posttranslational modifications of ApoC3

MS/MS fragments were analyzed using Lift-option of the MALDI-TOF/TOF mass-spectrometer. Calibrated and annotated spectra were subjected to the database search Swiss-Prot. (http://www.expasy.org) utilizing the software tool “Bruker Bio-Tool 3.2 and the “Mascot 2.2 search engine” (Matrix Science Ltd, London, UK).

***Ex vivo* guanidinylation of ApoC3**

Ex vivo guanidinylation of ApoC3 (50 µg) was performed by adapting a recently described method (Rueth et al., 2015). Briefly, 50 µg/mL aqueous ApoC3 solution was incubated with 1 mM o-methylisourea-bisulfate solution (Sigma Aldrich, Germany), guanidinehydrochloride solution (Sigma Aldrich, Germany) or urea (Sigma Aldrich, Germany) for 24h at room

temperature. After incubation, the reaction mixtures were diluted and dialyzed against PBS. The modified protein was digested by trypsin and analyzed by matrix-assisted-laser-desorption/ionization-time-of-flight-mass spectrometry (MALDI-TOF-TOF) as described above.

2D proteomic analyses in tissues

Sections of FFPE (formalin-fixed, paraffin-embedded) mice heart were mounted on specially coated slides (indium-tin-oxide coated Slides, Bruker Daltonic, Bremen, Germany).The heart sections were dewaxed, tryptically digested and coated with Matrix (α-cyano-4-hydroxycinnamic acid, Bruker Daltonic, Bremen, Germany) for the MALDI TOF/ TOF measurement.

Sections of fresh frozen mice kidney were mounted on specially coated slides (indium-tin-oxide coated Slides, Bruker Daltonic, Bremen, Germany). Before mounting, the slides were additionally coated with polylysine. The kidney sections were tryptically digested and coated with Matrix (α-cyano-4-hydroxycinnamic acid, Bruker Daltonic, Bremen, Germany) for the MALDI TOF/TOF measurement.

The coating with trypsin and matrix were made with a sprayer for MALDI Imaging (HTX TM-Sprayer: TMSP-M3, HTX Technologies, Chapel Hill, USA). The sections were measured with Rapiflex (Bruker Daltonics, Bremen, Germany) in positive reflector mode, a mass range of 500-3200 Dalton and a grid size of 30 µm and the imaging analyze were made with SCiLS Lab 2020b (Bruker Daltonics, Bremen, Germany). Also, the MS/MS spectra were created with the rapiflex, followed by a database search (SwissProt) using the Mascot 2.2 search engine (Matrix Science Inc, Boston, MA) and Bruker Bio-Tool 3.2 software (Bruker Daltonics, Bremen, Germany).

Isolation of Monocytes

PBMCs were isolated from peripheral blood of healthy subjects using Ficoll gradient centrifugation. A total of $1x10^6$ cells were seeded in 96 well plates for enzyme-linked

immunosorbent assay (ELISA) in full medium (RPMI GlutaMax, 10 % Fetal bovine serum, penicillin/streptomycin, and 10 mM HEPES). After one hour, non-adherent cells were removed and the medium was changed to starvation medium (RPMI GlutaMax, penicillin/streptomycin, and 10 mM HEPES). Cells were incubated with nApoC3 or gApoC3 (50 µg/mL) for 16 hours.

ELISA

Cytokine concentrations in supernatants from human monocytes were determined using commercially available ELISA kits according to manufacturer's instructions.

Electron Spin Resonance (ESR) spectroscopy

The spin probe 1-hydroxy-3-methoxycarbonyl-2,2,5,5-tetramethylpyrrolidine (CMH) was used to determine superoxide production. Cells were placed in 200 µl Krebs-Hepes buffer containing 25 µM deferoxamine (Noxygen) and 5 µM diethyldithiocarbamate (DETC). Afterwards, the spin probe CMH (200 µM, Noxygen) was added and cells were incubated with ApoC3 (50 µg/mL) or LPS (100 ng/mL) for 1 hr at 37°C/5 % CO_2. After incubation, supernatant was transferred into new 96 well plates and stored at 4 °C. ESR spectra of 50 µl of the supernatants were recorded using a Bruker e-scan spectrometer (Bruker Biospin) with the following settings: center field 3484.5 g, microwave power 18.11 mW, modulation amplitude 2.3 G, sweep time 5.24 s, field sweep 16 G.

Fluorescent labeling of ApoC3 using Atto-488

1 mg of ApoC3 was diluted in PBS to achieve a final volume of 170 µl. Atto-488 diluted in sodium bicarbonate buffer (1.0 M, pH 8.5) was added and the suspension was incubated for 1 hr at room temperature. After incubation, Atto-488-labeled ApoC3 was purified using gel filtration.

Flow cytometry

HEK293 cells co-transfected with human *Tlr2* or *Tlr4* and SEAP genes or PBMCs were incubated with Atto-488-labeled ApoC3 (50 µg/mL) for 1 hr. Cells were washed three times with PBS and then subjected to analysis by flow cytometry (BD FACSCanto II). Binding/internalization of Atto-488-ApoC3 was analyzed by using FlowJo software.

Histology and immunofluorescence

Hematoxyline/eosine, Sirius red, and Gomori Trichrome stainings were performed according to standard protocols. Images were analyzed using a Zeiss Axio Imager 2 and the software ZEN. Ly6G, F4/80 and DKK3 expression was quantified using immunofluorescence microscopy. The Ly6G-, F4/80-, and DKK3-positive area was quantified using Image J. Investigators were blinded for the respective treatment groups.

Experimental myocardial infarction model

All experiments were approved by the government of North Rhine-Westphalia (Germany). Male 6-week-old C57Bl/6J mice were obtained from Janvier Labs and placed in a 12 h day-night cycle with unlimited supply of food and water in the animal facility of the University Hospital of the RWTH Aachen University. After a one-week adaptation to our facility, permanent ligation of the left anterior descending artery (LAD) was performed to induce myocardial infarction. Mice were anesthetized with Ketamin (100 mg/kg)/Xylazin (10 mg/kg) and temgesic was used for analgesia. After intubation mice were ventilated with a stroke volume of 200 µl and a respiration rate of 120 strokes per minute. Chest was opened via the fourth intercostal space at the left upper sternal border through a small incision and AMI was induced by LAD ligation. Control mice underwent a sham operation in which the pericardium was opened. 7 days and 28 days after surgery, mice were anesthetized as described before and sacrificed by cervical dislocation. Heart tissue was fixed in 4% paraformaldehyde overnight, embedded in paraffin and 5 µm sections were collected.

Adenine diet in mice

Mice were subjected to an adenine diet (0.2 %, Altromin) to induce kidney damage. Control mice were fed with a normal chow diet (Altromin).

Humanized mice

Isolation of total PBMCs from peripheral blood of healthy donors was performed as described below. Isolated PBMCs were subjected to magnetic cell separation using LS columns and human CD14 microbeads (Miltenyi Biotec). Afterwards, purity of the monocytes was determined by using flow cytometry after staining with CD14 PerCp/Cy5.5 (data not shown). Cells were immediately used for transplantation into NOD-SCID mice as described above.

Murine carotid injury model

Murine carotid injury model was performed as described previously (Speer et al., 2013a). Briefly, NOD-SCID mice were anaesthetized with isofluorane. Left common carotid artery was injured with a bipolar microregulator. An electric current of 2 W was applied for 2 seconds to each millimeter of carotid artery over a total length of exactly 4 mm. Afterwards, CD14+ human monocytes were injected via tail vein together with nApoC3 or gApoC3 (50 µg/mL blood volume). One week later, mice were perfused with Evans blue to stain the de-endothelialized area of the carotid arteries. Afterwards, carotid arteries were excised and re-endothelialized area was quantified.

Murine unilateral ureter ligation model

Unilateral ureter ligation was performed in NOD-SCID mice anaesthetized with isoflurane. After low middle-left incision on the abdominal side, the left ureter was ligated with 2/0 prolene. Afterwards, 10^7 CD14+ human monocytes were injected into NOD-SCID mice via tail vein together with nApoC3 or gApoC3 (50 µg/mL blood volume). Five days later, mice were euthanized and damage kidneys were subjected for microscopic analyses.

Quantification and Statistical Analysis

In the experimental studies, bars and whiskers represent mean±SEM. Statistical differences were examined using Student's t test or one-way analysis of variance (ANOVA) followed by Dunnett's post-hoc test to adjust for multiple comparisons.

In the clinical studies, continuous data are presented as mean±SD when normally distributed or as median and interquartile range (IQR) for variables with skewed distribution. Statistical differences between continuous variables were determined using one-way ANOVA, Kruskal–Wallis test, or chi-squared test for categorical variables.

The non-linear associations between ApoC3 guanidinylation intensity and mortality, combined cardiovascular, or renal endpoint were analyzed using restricted cubic spline plots with three knots (0.000, 0.007, 0.162). Analyses were adjusted for age, sex, prevalent cardiovascular disease, body mass index, systolic blood pressure, smoking status, diabetes mellitus, eGFR, and albuminuria. Additionally, Cox regression analyses were performed for the aforementioned endpoints using ApoC3 guanidinylation intensity divided in tertiles and adjustments as indicated in the respective tables. Moreover, the association between ApoC3 and triglyceride plasma levels divided in tertiles and mortality, the cardiovascular or the renal endpoint was determined by Cox regression analyses.

To assess the association between ApoC3 guanidinylation intensity and annual changes of eGFR during follow-up, group-based trajectory modelling of eGFR was performed using the STATA package 'traj'. This approach is based on the SAS PROC TRAJ macro (Nagin et al., 2018), which fits a semiparametric (discrete mixture) model for longitudinal data using maximum likelihood methods. We used the Bayesian information criterion (BIC) to establish the optimal number of groups. We then performed multinominal logistic regression analyses to determine the association between ApoC3 guanidinylation intensity and assignment to the different trajectory groups using the group 1 as reference. Also, these analyses were adjusted for age, sex, prevalent cardiovascular disease, body mass index, systolic blood pressure, smoking status, diabetes mellitus, eGFR, and albuminuria.

A two-sided *P* value of less than 0.05 was considered statistically significant. Statistical analyses were performed using SPSS version 25.0 and STATA IC 15 with the packages postrcspline and traj.

References

Avall, K., Ali, Y., Leibiger, I.B., Leibiger, B., Moede, T., Paschen, M., Dicker, A., Dare, E., Kohler, M., Ilegems, E.*, et al.* (2015). Apolipoprotein CIII links islet insulin resistance to beta-cell failure in diabetes. Proc Natl Acad Sci U S A *112*, E2611-2619.

Breitkopf, D.M., Jankowski, V., Ohl, K., Hermann, J., Hermert, D., Tenbrock, K., Liu, X., Martin, I.V., Wang, J., Groll, F.*, et al.* (2020). The YB-1:Notch-3 axis modulates immune cell responses and organ damage in systemic lupus erythematosus. Kidney Int *97*, 289-303.

Chronic Kidney Disease Prognosis Consortium, Matsushita, K., van der Velde, M., Astor, B.C., Woodward, M., Levey, A.S., de Jong, P.E., Coresh, J., and Gansevoort, R.T. (2010). Association of estimated glomerular filtration rate and albuminuria with all-cause and cardiovascular mortality in general population cohorts: a collaborative meta-analysis. Lancet *375*, 2073-2081.

Cullen, M.E., Yuen, A.H., Felkin, L.E., Smolenski, R.T., Hall, J.L., Grindle, S., Miller, L.W., Birks, E.J., Yacoub, M.H., and Barton, P.J. (2006). Myocardial expression of the arginine:glycine amidinotransferase gene is elevated in heart failure and normalized after recovery: potential implications for local creatine synthesis. Circulation *114*, I16-20.

Deshmukh, D.R., Ghole, V.S., Marescau, B., and De Deyn, P.P. (1997). Effect of endotoxemia on plasma and tissue levels of nitric oxide metabolites and guanidino compounds. Arch Physiol Biochem *105*, 32-37.

G. B. D. Disease Injury Incidence Prevalence Collaborators (2018). Global, regional, and national incidence, prevalence, and years lived with disability for 354 diseases and injuries for 195 countries and territories, 1990-2017: a systematic analysis for the Global Burden of Disease Study 2017. Lancet *392*, 1789-1858.

Gajjala, P.R., Fliser, D., Speer, T., Jankowski, V., and Jankowski, J. (2015). Emerging role of post-translational modifications in chronic kidney disease and cardiovascular disease. Nephrol Dial Transplant *30*, 1814-1824.

Gaudet, D., Alexander, V.J., Baker, B.F., Brisson, D., Tremblay, K., Singleton, W., Geary, R.S., Hughes, S.G., Viney, N.J., Graham, M.J.*, et al.* (2015). Antisense Inhibition of Apolipoprotein C-III in Patients with Hypertriglyceridemia. N Engl J Med *373*, 438-447.

Gaudet, D., Brisson, D., Tremblay, K., Alexander, V.J., Singleton, W., Hughes, S.G., Geary, R.S., Baker, B.F., Graham, M.J., Crooke, R.M.*, et al.* (2014). Targeting APOC3 in the familial chylomicronemia syndrome. N Engl J Med *371*, 2200-2206.

Gordts, P.L., Nock, R., Son, N.H., Ramms, B., Lew, I., Gonzales, J.C., Thacker, B.E., Basu, D., Lee, R.G., Mullick, A.E.*, et al.* (2016). ApoC-III inhibits clearance of triglyceride-rich lipoproteins through LDL family receptors. J Clin Invest *126*, 2855-2866.

Graham, M.J., Lee, R.G., Bell, T.A., 3rd, Fu, W., Mullick, A.E., Alexander, V.J., Singleton, W., Viney, N., Geary, R., Su, J.*, et al.* (2013). Antisense oligonucleotide inhibition of apolipoprotein

C-III reduces plasma triglycerides in rodents, nonhuman primates, and humans. Circ Res *112*, 1479-1490.

Jensen, M.K., Aroner, S.A., Mukamal, K.J., Furtado, J.D., Post, W.S., Tsai, M.Y., Tjonneland, A., Polak, J.F., Rimm, E.B., Overvad, K.*, et al.* (2018). High-Density Lipoprotein Subspecies Defined by Presence of Apolipoprotein C-III and Incident Coronary Heart Disease in Four Cohorts. Circulation *137*, 1364-1373.

Jorgensen, A.B., Frikke-Schmidt, R., Nordestgaard, B.G., and Tybjaerg-Hansen, A. (2014). Loss-of-function mutations in APOC3 and risk of ischemic vascular disease. N Engl J Med *371*, 32-41.

KDIGO (2012). KDIGO 2012 Clinical Practice Guideline for the Evaluation and Management of Chronic Kidney Disease. Kidney Int *Supplement 3*, 1-150.

Khetarpal, S.A., Zeng, X., Millar, J.S., Vitali, C., Somasundara, A.V.H., Zanoni, P., Landro, J.A., Barucci, N., Zavadoski, W.J., Sun, Z.*, et al.* (2017). A human APOC3 missense variant and monoclonal antibody accelerate apoC-III clearance and lower triglyceride-rich lipoprotein levels. Nat Med *23*, 1086-1094.

Martinelli, N., Baroni, M., Castagna, A., Lunghi, B., Stefanoni, F., Tosi, F., Croce, J., Udali, S., Woodhams, B., Girelli, D.*, et al.* (2019). Apolipoprotein C-III Strongly Correlates with Activated Factor VII-Anti-Thrombin Complex: An Additional Link between Plasma Lipids and Coagulation. Thrombosis and haemostasis *119*, 192-202.

Morton, A.M., Koch, M., Mendivil, C.O., Furtado, J.D., Tjonneland, A., Overvad, K., Wang, L., Jensen, M.K., and Sacks, F.M. (2018). Apolipoproteins E and CIII interact to regulate HDL metabolism and coronary heart disease risk. JCI Insight *3*.

Nagin, D.S., Jones, B.L., Passos, V.L., and Tremblay, R.E. (2018). Group-based multi-trajectory modeling. Stat Methods Med Res *27*, 2015-2023.

Ortiz, A., Covic, A., Fliser, D., Fouque, D., Goldsmith, D., Kanbay, M., Mallamaci, F., Massy, Z.A., Rossignol, P., Vanholder, R.*, et al.* (2014). Epidemiology, contributors to, and clinical trials of mortality risk in chronic kidney failure. Lancet *383*, 1831-1843.

Petersen, K.F., Dufour, S., Hariri, A., Nelson-Williams, C., Foo, J.N., Zhang, X.M., Dziura, J., Lifton, R.P., and Shulman, G.I. (2010). Apolipoprotein C3 gene variants in nonalcoholic fatty liver disease. N Engl J Med *362*, 1082-1089.

Pollin, T.I., Damcott, C.M., Shen, H., Ott, S.H., Shelton, J., Horenstein, R.B., Post, W., McLenithan, J.C., Bielak, L.F., Peyser, P.A.*, et al.* (2008). A null mutation in human APOC3 confers a favorable plasma lipid profile and apparent cardioprotection. Science *322*, 1702-1705.

Rueth, M., Lemke, H.D., Preisinger, C., Krieter, D., Theelen, W., Gajjala, P., Devine, E., Zidek, W., Jankowski, J., and Jankowski, V. (2015). Guanidinylations of albumin decreased binding capacity of hydrophobic metabolites. Acta physiologica *215*, 13-23.

Schuett, K., Savvaidis, A., Maxeiner, S., Lysaja, K., Jankowski, V., Schirmer, S.H., Dimkovic, N., Boor, P., Kaesler, N., Dekker, F.W.*, et al.* (2017). Clot Structure: A Potent Mortality Risk Factor in Patients on Hemodialysis. J Am Soc Nephrol *28*, 1622-1630.

Speer, T., Owala, F.O., Holy, E.W., Zewinger, S., Frenzel, F.L., Stahli, B.E., Razavi, M., Triem, S., Cvija, H., Rohrer, L.*, et al.* (2014a). Carbamylated low-density lipoprotein induces endothelial dysfunction. Eur Heart J *35*, 3021-3032.

Speer, T., Rohrer, L., Blyszczuk, P., Shroff, R., Kuschnerus, K., Krankel, N., Kania, G., Zewinger, S., Akhmedov, A., Shi, Y.*, et al.* (2013a). Abnormal high-density lipoprotein induces endothelial dysfunction via activation of Toll-like receptor-2. Immunity *38*, 754-768.

Speer, T., Shroff, R., Colin, S., Charakida, M., Zewinger, S., Staels, B., Chinetti-Gbaguidi, G., Hettrich, I., Rohrer, L., O'Neill, F.*, et al.* (2014b). HDL in Children with CKD Promotes Endothelial Dysfunction and an Abnormal Vascular Phenotype. J Am Soc Nephrol *25*, 2658-2668.

Speer, T., Zewinger, S., and Fliser, D. (2013b). Uraemic dyslipidaemia revisited: role of high-density lipoprotein. Nephrol Dial Transplant *28*, 2456-2463.

TG and HDL Working Group of the Exome Sequencing Project, N.H.L., Blood, I., Crosby, J., Peloso, G.M., Auer, P.L., Crosslin, D.R., Stitziel, N.O., Lange, L.A., Lu, Y., Tang, Z.Z.*, et al.* (2014). Loss-of-function mutations in APOC3, triglycerides, and coronary disease. N Engl J Med *371*, 22-31.

Urpi-Sarda, M., Almanza-Aguilera, E., Llorach, R., Vazquez-Fresno, R., Estruch, R., Corella, D., Sorli, J.V., Carmona, F., Sanchez-Pla, A., Salas-Salvado, J.*, et al.* (2019). Non-targeted metabolomic biomarkers and metabotypes of type 2 diabetes: A cross-sectional study of PREDIMED trial participants. Diabetes Metab *45*, 167-174.

Wang, Z., Nicholls, S.J., Rodriguez, E.R., Kummu, O., Horkko, S., Barnard, J., Reynolds, W.F., Topol, E.J., DiDonato, J.A., and Hazen, S.L. (2007). Protein carbamylation links inflammation, smoking, uremia and atherogenesis. Nat Med *13*, 1176-1184.

Witztum, J.L., Gaudet, D., Freedman, S.D., Alexander, V.J., Digenio, A., Williams, K.R., Yang, Q., Hughes, S.G., Geary, R.S., Arca, M.*, et al.* (2019). Volanesorsen and Triglyceride Levels in Familial Chylomicronemia Syndrome. N Engl J Med *381*, 531-542.

Wolska, A., Lo, L., Sviridov, D.O., Pourmousa, M., Pryor, M., Ghosh, S.S., Kakkar, R., Davidson, M., Wilson, S., Pastor, R.W.*, et al.* (2020). A dual apolipoprotein C-II mimetic-apolipoprotein C-III antagonist peptide lowers plasma triglycerides. Science translational medicine *12*.

Zewinger, S., Drechsler, C., Kleber, M.E., Dressel, A., Riffel, J., Triem, S., Lehmann, M., Kopecky, C., Saemann, M.D., Lepper, P.M.*, et al.* (2015). Serum amyloid A: high-density lipoproteins interaction and cardiovascular risk. Eur Heart J *36*, 3007-3016.

Zewinger, S., Kleber, M.E., Rohrer, L., Lehmann, M., Triem, S., Jennings, R.T., Petrakis, I., Dressel, A., Lepper, P.M., Scharnagl, H.*, et al.* (2017). Symmetric dimethylarginine, high-density lipoproteins and cardiovascular disease. Eur Heart J *38*, 1597-1607.

Zewinger, S., Rauen, T., Rudnicki, M., Federico, G., Wagner, M., Triem, S., Schunk, S.J., Petrakis, I., Schmit, D., Wagenpfeil, S.*, et al.* (2018). Dickkopf-3 (DKK3) in Urine Identifies Patients with Short-Term Risk of eGFR Loss. J Am Soc Nephrol *29*, 2722-2733.

Zewinger, S., Reiser, J., Jankowski, V., Alansary, D., Hahm, E., Triem, S., Klug, M., Schunk, S.J., Schmit, D., Kramann, R.*, et al.* (2020). Apolipoprotein C3 induces inflammation and organ damage by alternative inflammasome activation. Nat Immunol *21*, 30-41.

Zewinger, S., Speer, T., Kleber, M.E., Scharnagl, H., Woitas, R., Lepper, P.M., Pfahler, K., Seiler, S., Heine, G.H., März, W.*, et al.* (2014). HDL cholesterol is not associated with lower mortality in patients with kidney dysfunction. J Am Soc Nephrol *25*, 1073-1082.

Zheng, C., Azcutia, V., Aikawa, E., Figueiredo, J.L., Croce, K., Sonoki, H., Sacks, F.M., Luscinskas, F.W., and Aikawa, M. (2013). Statins suppress apolipoprotein CIII-induced vascular endothelial cell activation and monocyte adhesion. Eur Heart J *34*, 615-624.

Figure 1

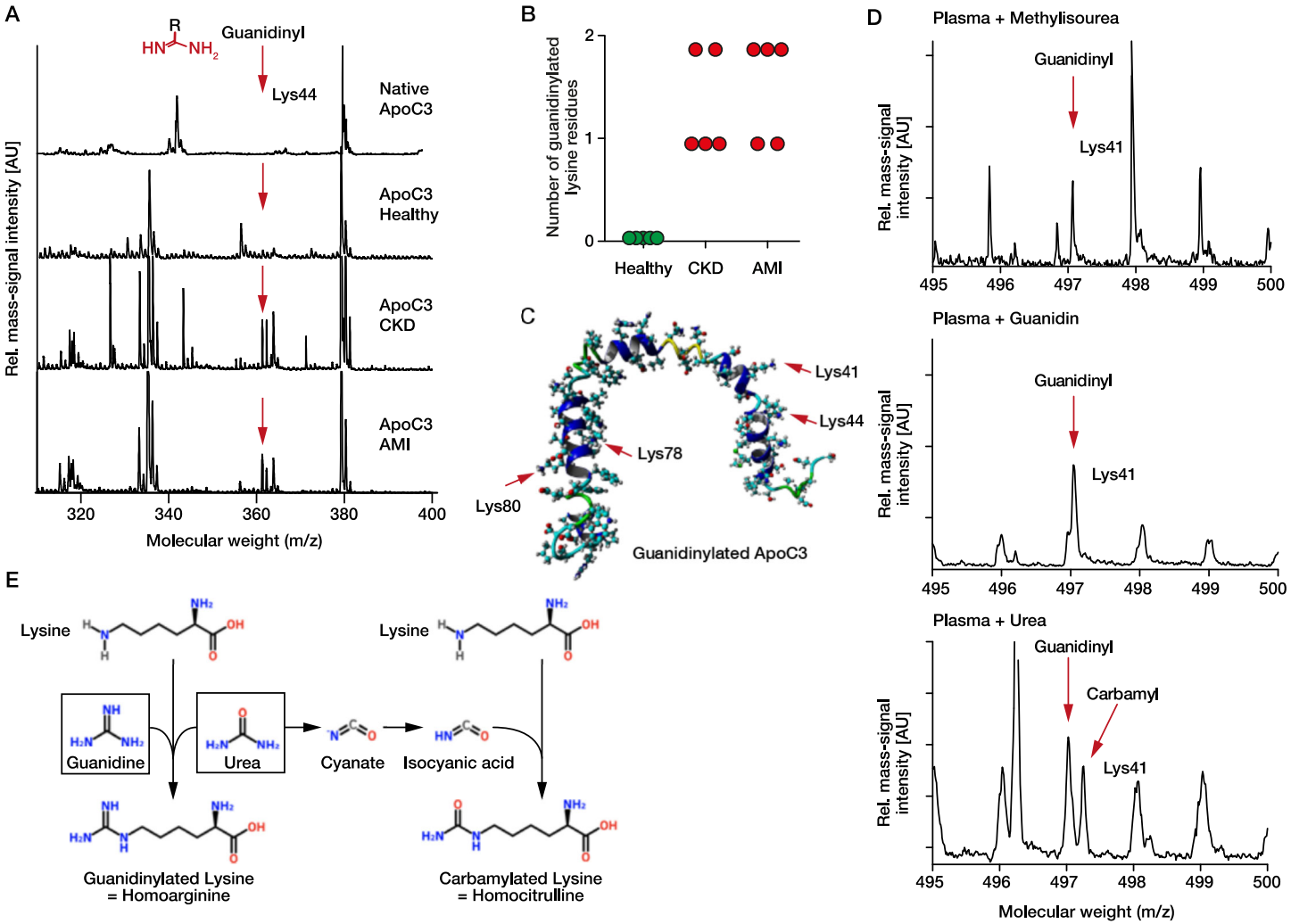
A
Guanidinyl
Lys44
Native ApoC3
ApoC3 Healthy
ApoC3 CKD
ApoC3 AMI
Rel. mass-signal intensity [AU]
320
340
360
380
400
Molecular weight (m/z)
B
Number of guanidinylated lysine residues
Healthy
CKD
AMI
C
Lys41
Lys44
Lys78
Lys80
Guanidinylated ApoC3
D
Plasma + Methylisourea
Guanidinyl
Lys41
Plasma + Guanidin
Guanidinyl
Lys41
Plasma + Urea
Guanidinyl
Carbamyl
Lys41
Rel. mass-signal intensity [AU]
495
496
497
498
499
500
Molecular weight (m/z)
E
Lysine
Lysine
Guanidine
Urea
Cyanate
Isocyanic acid
Guanidinylated Lysine
= Homoarginine
Carbamylated Lysine
= Homocitrulline

Figure 2

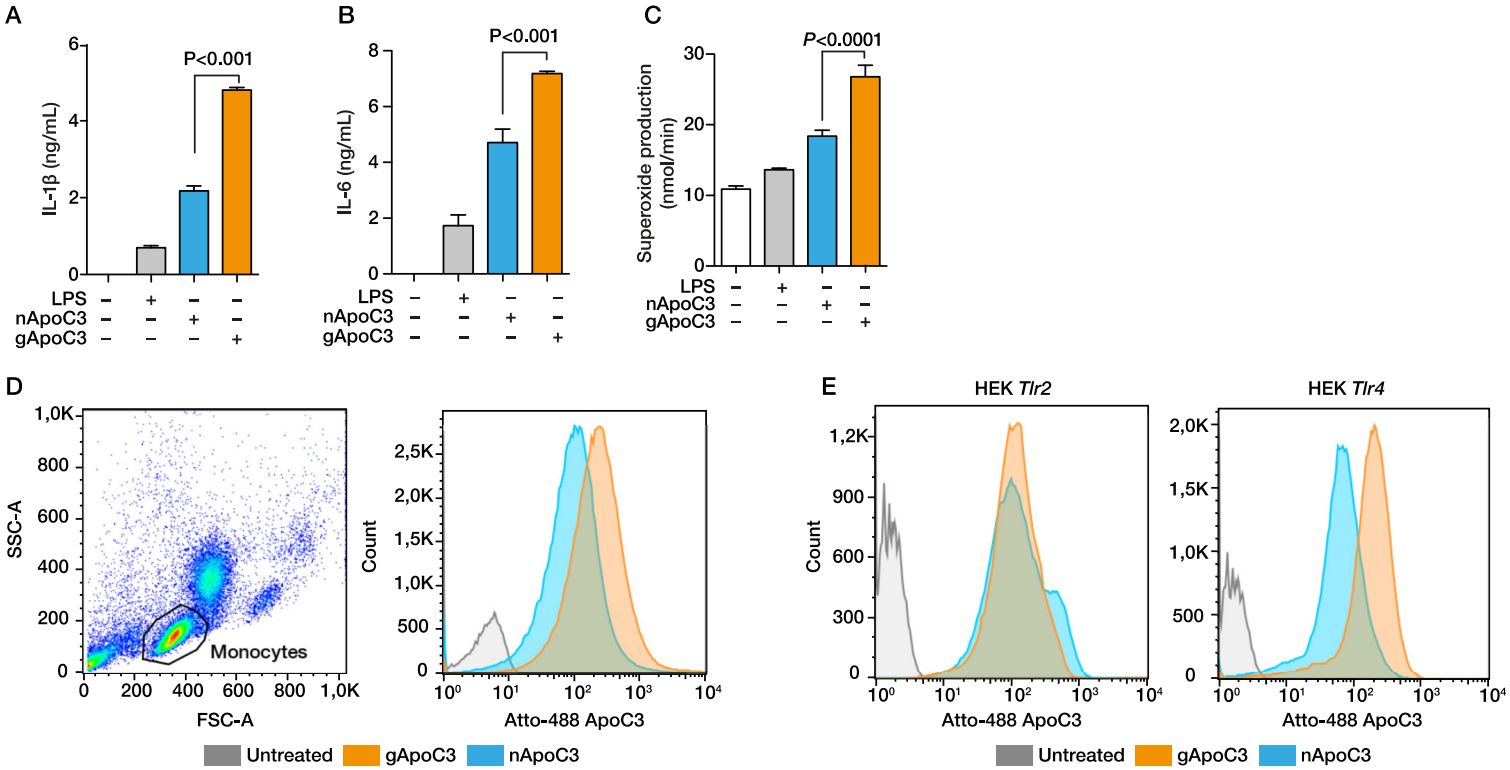
A
IL-1β (ng/mL)
P<0.001
LPS
nApoC3
gApoC3
B
IL-6 (ng/mL)
P<0.001
C
Superoxide production (nmol/min)
P<0.0001
D
SSC-A
FSC-A
Monocytes
Count
Atto-488 ApoC3
Untreated
gApoC3
nApoC3
E
HEK Tlr2
HEK Tlr4
Count
Atto-488 ApoC3
Untreated
gApoC3
nApoC3

Figure 3

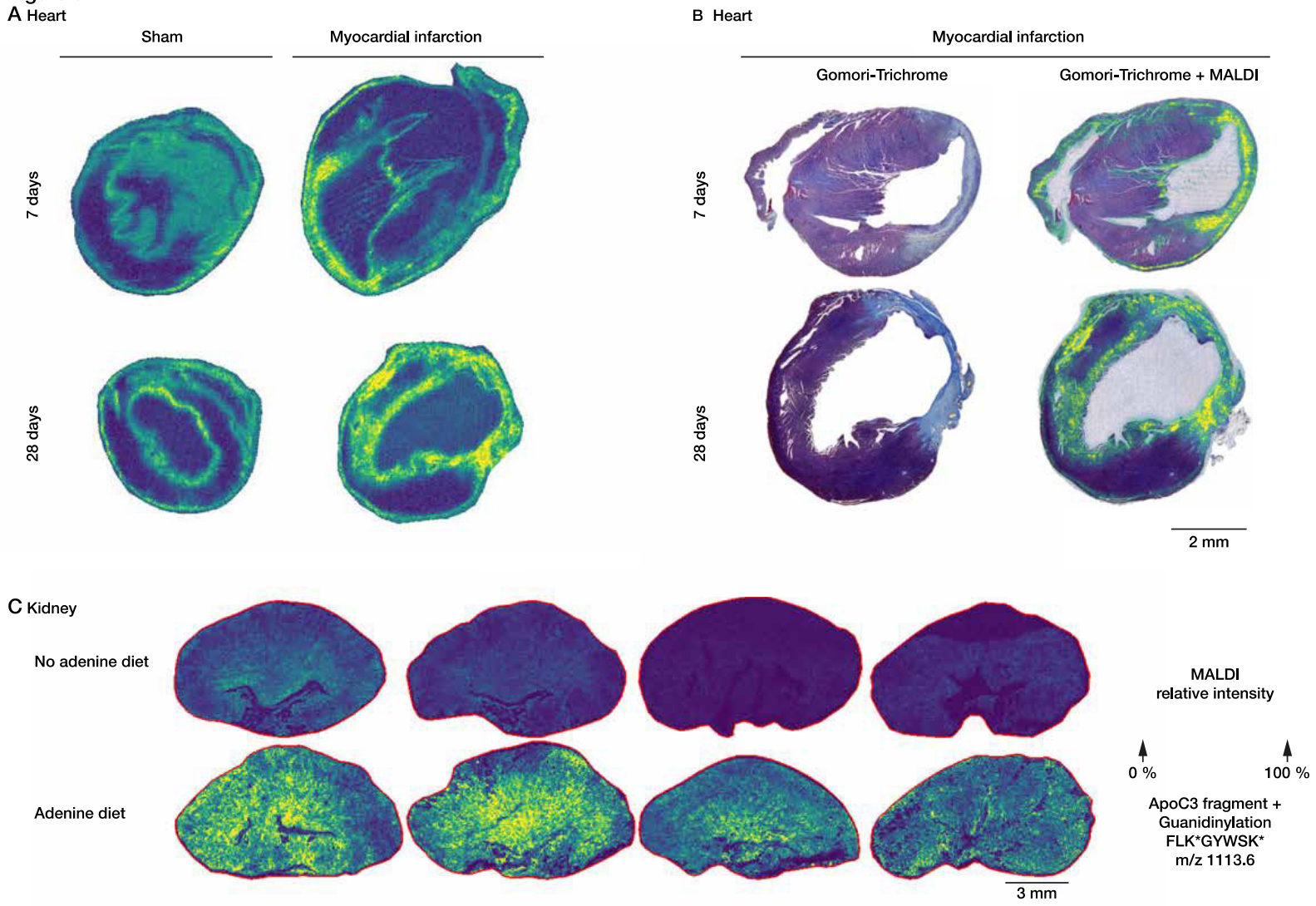
A Heart
Sham
Myocardial infarction
7 days
28 days
B Heart
Myocardial infarction
Gomori-Trichrome
Gomori-Trichrome + MALDI
7 days
28 days
2 mm
C Kidney
No adenine diet
Adenine diet
3 mm
MALDI
relative intensity
0 %
100 %
ApoC3 fragment +
Guanidinylation
FLK*GYWSK*
m/z 1113.6

Figure 4

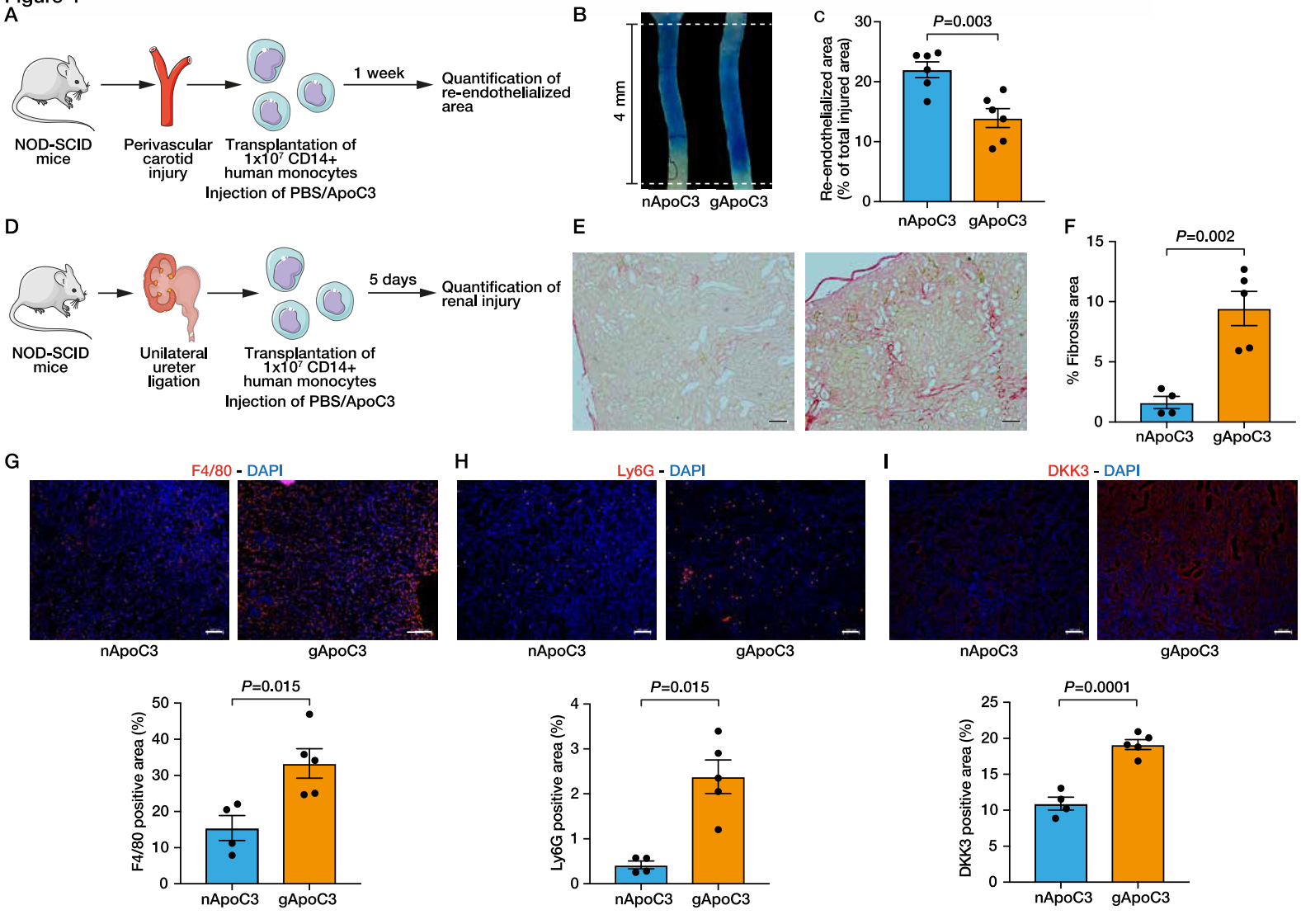
A
NOD-SCID mice
Perivascular carotid injury
Transplantation of 1x10⁷ CD14+ human monocytes
Injection of PBS/ApoC3
1 week
Quantification of re-endothelialized area
B
4 mm
nApoC3
gApoC3
C
P=0.003
Re-endothelialized area (% of total injured area)
30
20
10
0
nApoC3
gApoC3
D
NOD-SCID mice
Unilateral ureter ligation
Transplantation of 1x10⁷ CD14+ human monocytes
Injection of PBS/ApoC3
5 days
Quantification of renal injury
E
F
P=0.002
% Fibrosis area
15
10
5
0
nApoC3
gApoC3
G
F4/80 - DAPI
nApoC3
gApoC3
P=0.015
F4/80 positive area (%)
50
40
30
20
10
0
nApoC3
gApoC3
H
Ly6G - DAPI
nApoC3
gApoC3
P=0.015
Ly6G positive area (%)
4
3
2
1
0
nApoC3
gApoC3
I
DKK3 - DAPI
nApoC3
gApoC3
P=0.0001
DKK3 positive area (%)
25
20
15
10
5
0
nApoC3
gApoC3

Figure 5

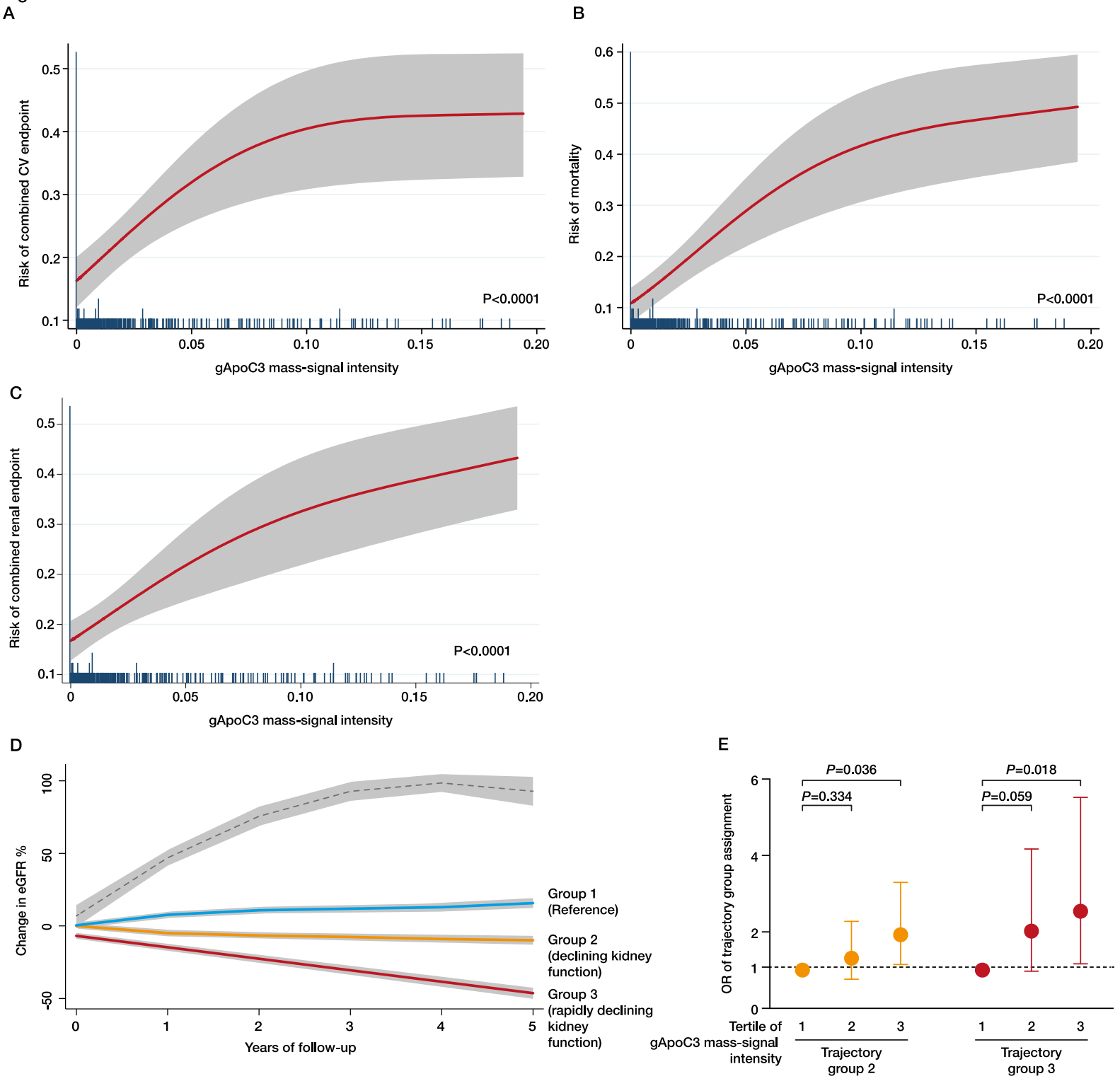
A
Risk of combined CV endpoint
0.5
0.4
0.3
0.2
0.1
P<0.0001
0
0.05
0.10
0.15
0.20
gApoC3 mass-signal intensity
B
Risk of mortality
0.6
0.5
0.4
0.3
0.2
0.1
P<0.0001
0
0.05
0.10
0.15
0.20
gApoC3 mass-signal intensity
C
Risk of combined renal endpoint
0.5
0.4
0.3
0.2
0.2
0.1
P<0.0001
0
0.05
0.10
0.15
0.20
gApoC3 mass-signal intensity
D
Change in eGFR %
100
50
0
-50
0
1
2
3
4
5
Years of follow-up
Group 1
(Reference)
Group 2
(declining kidney
function)
Group 3
(rapidly declining
kidney
function)
E
P=0.036
P=0.334
P=0.018
P=0.059
OR of trajectory group assignment
6
4
2
1
0
Tertile of
gApoC3 mass-signal
intensity
1
2
3
1
2
3
Trajectory
group 2
Trajectory
group 3

Figure S1

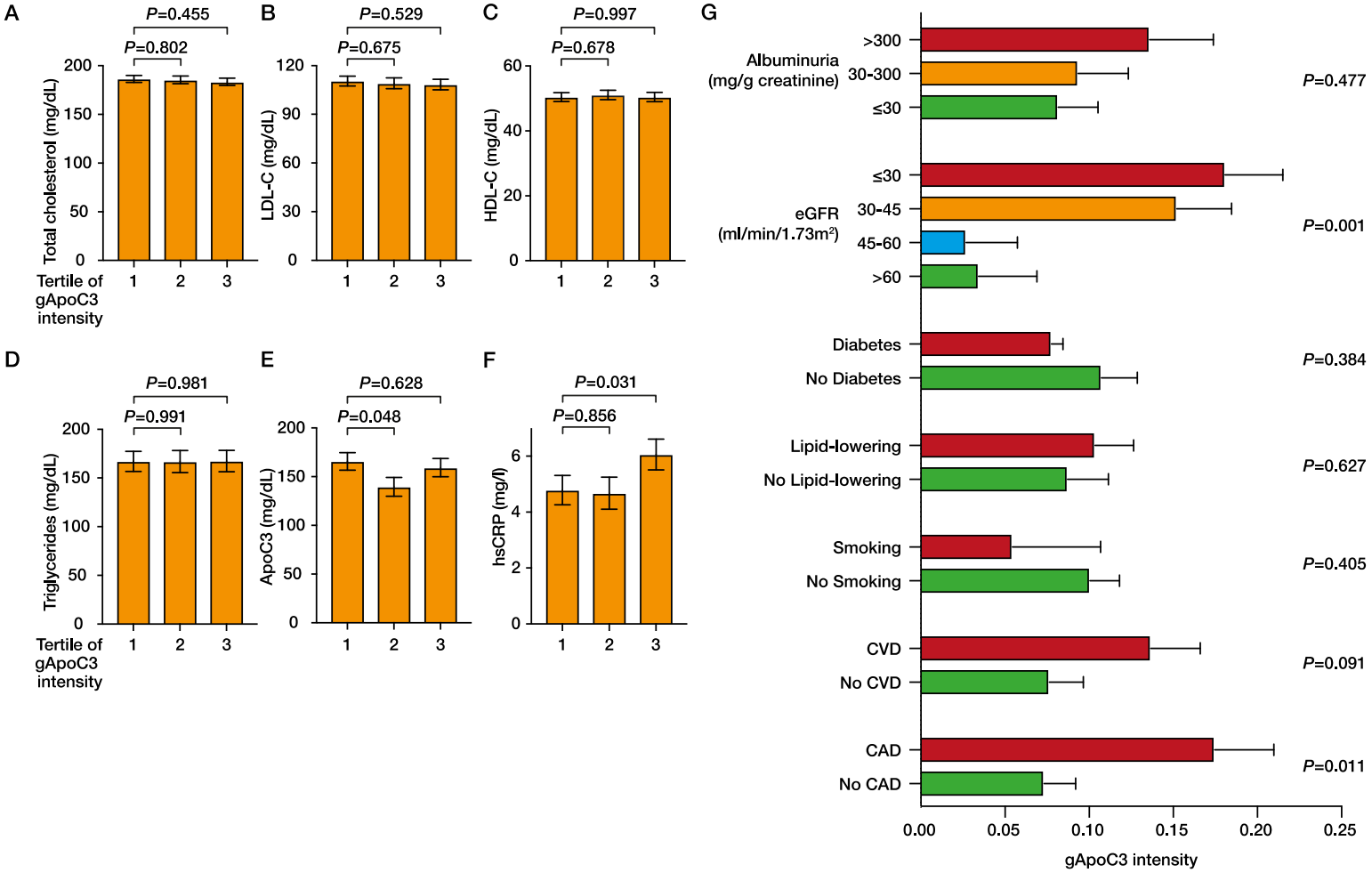
A
P=0.455
P=0.802
Total cholesterol (mg/dL)
200
150
100
50
0
Tertile of gApoC3 intensity
1
2
3
B
P=0.529
P=0.675
LDL-C (mg/dL)
120
90
60
30
0
C
P=0.997
P=0.678
HDL-C (mg/dL)
60
40
20
0
D
P=0.981
P=0.991
Triglycerides (mg/dL)
E
P=0.628
P=0.048
ApoC3 (mg/dL)
F
P=0.031
P=0.856
hsCRP (mg/l)
6
4
2
G
Albuminuria (mg/g creatinine)
>300
30-300
≤30
P=0.477
eGFR (ml/min/1.73m²)
≤30
30-45
45-60
>60
P=0.001
Diabetes
No Diabetes
P=0.384
Lipid-lowering
No Lipid-lowering
P=0.627
Smoking
No Smoking
P=0.405
CVD
No CVD
P=0.091
CAD
No CAD
P=0.011
0.00
0.05
0.10
0.15
0.20
0.25
gApoC3 intensity